RSC Advances

PAPER

View Article Online
View Journal | View Issue

Cite this: *RSC Adv.*, 2017, **7**, 3443

Synthesis of Pd/SBA-15 catalyst employing surface-bonded vinyl as a reductant and its application in the hydrogenation of nitroarenes†

Ying Duan,[ab] Min Zheng,[a] Dongmi Li,[a] Dongsheng Deng,[a] Cuicui Wu[a] and Yanliang Yang*[a]

Received 15th November 2016
Accepted 16th December 2016

DOI: 10.1039/c6ra26811k

www.rsc.org/advances

The Pd/SBA-15 catalyst was synthesised through the reduction of $PdCl_2$ by the surface-bonded vinyl group on vinyl-functionalized SBA-15, which was prepared *via* co-polymerization. XRD and XPS characterization confirmed the successful reduction of Pd(II) to Pd(0). Pd/SBA-15 showed a narrow palladium particle-size distribution of about 5–6 nm in the TEM image. The Pd/SBA-15 catalyst was effective for the hydrogenation of aromatic nitro compounds with zero-order kinetics, and the TOF for the hydrogenation of nitrobenzene was 1124 h^{-1} at 313 K and 1 atm H_2. A steric effect was observed for the substituted nitroarenes.

Introduction

Owning to their unique structures and high activity, the synthesis of supported palladium nanoparticles is of great significance in heterogeneous catalysis.[1–3] Numerous methods have been developed to prepare these catalysts, which have been widely used in hydrogenation,[4–8] hydrogenolysis,[9–12] decarbonylation,[13,14] coupling reactions,[15–18] oxidation,[19] and so on.[20–23] The synthesis of supported palladium nanoparticles usually involves a palladium salt as the palladium source to be reduced to palladium(0) by a reducing agent, such as H_2, formic acid or glycol. Since the palladium salt and the reducing agent do not often symmetrically distribute on the supports, additional means should be taken to acquire a uniform distribution of the palladium nanoparticles. For example, PVP is usually used as a protective agent to stabilize the palladium nanoparticles.[24]

An interesting method for the preparation of supported palladium nanoparticles is to employ a reducing agent uniformly bound to the surface of the supports. The palladium salt then could only be reduced on the surface of the supports and the resulting palladium nanoparticles will not enlarge as there are no more reducing agents nearby. Lu's group reported an example of the preparation of carbon spheres supported palladium using the surface groups as reducing agents.[25] A superior product with small (d = 7.66 nm, σ = 1.94 nm), homogeneously distributed Pd crystals was obtained. Li *et al.* first synthesized a Si–H functionalized phenyl-bridged periodic mesoporous organosilica (PMO).[26] Then, Pd nanoparticles were immobilized onto the PMO by a Si–H *in situ* reduction method. The resulting catalysts showed excellent catalytic activity and selectivity for the Ullmann reaction in water.

Anilines, which are important chemical raw materials, are widely applied for the synthesis of dyes, agrochemicals, polymers, pharmaceuticals, and other fine chemicals.[27,28] The conventional procedure for the production of aromatic amines is the reduction of the corresponding nitro derivatives. Therefore, it is highly significant to synthesize an appropriate catalyst with remarkable performance for this hydrogenation procedure.[29–32]

In this study, we report the preparation of SBA-15 with surface-bonded vinyl as a catalyst. Also, vinyl was used as a reducing agent for the synthesis of Pd/SBA-15. As illustrated in Scheme 1, $PdCl_2$ was reduced by the surface-bonded vinyl group to afford Pd(0), which is part of the Wacker reaction. Once vinyl is consumed, the palladium nanoparticles cannot grow bigger.

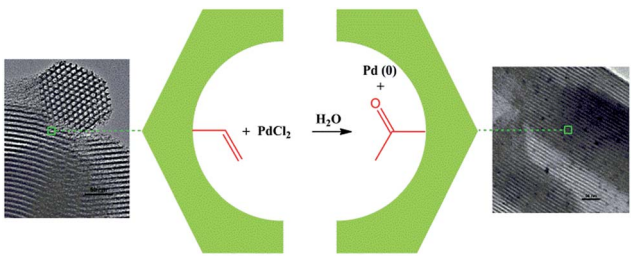

Scheme 1 The preparation of Pd/SBA-15 using surface-bonded vinyl as reductant.

[a]*Henan Key Laboratory of Function-Oriented Porous Material, College of Chemistry and Chemical Engineering, Luoyang Normal University, Luoyang 471934, P. R. China. E-mail: yangyl0410@126.com*

[b]*College of Food and Drug, Luoyang Normal University, Luoyang 471934, China*

† Electronic supplementary information (ESI) available. See DOI: 10.1039/c6ra26811k

As a result, the catalysts had a uniform distribution of palladium nanoparticles and were demonstrated to be effective in the hydrogenation of nitro aromatic compounds under a 1 atm H_2 atmosphere. The application of H_2 instead of $NaBH_4$ as a reducing agent offers the advantage that the product does not need to be extracted from the aqueous reaction medium. The other product is water, which together with the absence of salt, made this method clean and economical.

Material and methods

Materials

All the chemicals were of analytical grade and used as received. Poly(ethylene glycol)-*block*-poly(propylene glycol)-*block*-poly(-ethylene glycol) (P123, AR) was obtained from Sigma-Aldrich. Nitrobenzene, 2-nitrotoluene, 3-nitrotoluene, 4-nitrotoluene, 4-nitrophenylethane, 2-fluoronitrobenzene and aniline were purchased from Aladdin Chemistry Co. Ltd. Tetraethyl orthosilicate (TEOS), vinyltriethoxysilane (VTEO) and $PdCl_2$ were obtained from J&K Chemical Ltd. Deionized water was used in all the experiments. All the other reagents were commercially available.

Preparation of the catalysts

SBA-15. The mesoporous silica SBA-15 was synthesized according to the literature procedure reported by Zhao *et al.*[33] The typical procedure was as follows. P123 (4.00 g) was dissolved in an aqueous solution of HCl (2 mol L^{-1}, 125 mL) at 313 K. Next, a silicon source (TEOS, 8.50 g) was added dropwise into the solution and the mixture was stirred for 24 h at 313 K. Then, the mixture was transferred to an autoclave and maintained under heat for another 24 h at 373 K. The template was removed by refluxing in EtOH–HCl (100 : 1, 200 mL) three times. Then, the mixture was centrifuged and the solid was dried at 323 K in a vacuum overnight to afford SBA-15. Vinyl-functionalized SBA-15 was synthesized using a similar method,[35,36] except that TEOS (8.07 g) and VTEO (0.39 g) instead of TEOS were used as the silicon sources.

Pd/SBA-15. $PdCl_2$ was dissolved in HCl solution (0.1 mol L^{-1}) to form a yellow transparent $PdCl_2$ solution with 0.5 wt% Pd. Vinyl-functionalized SBA-15 (0.50 g) was dispersed in water (25 mL). Then, the solution of $PdCl_2$ (0.07 mmol $PdCl_2$) was added dropwise into the mixture prepared above under stirring at room temperature. After stirring for 4 h at room temperature, the solid was centrifuged and washed first with water (50 mL) three times

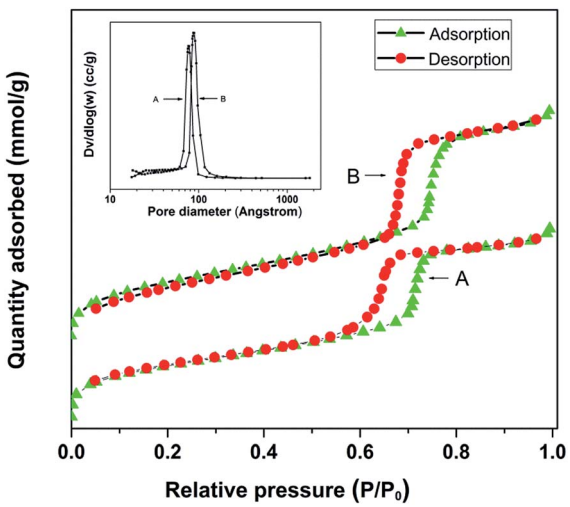

Fig. 1 N_2 adsorption/desorption isotherms of the as-synthesized SBA-15 (A) and Pd/SBA-15 (B).

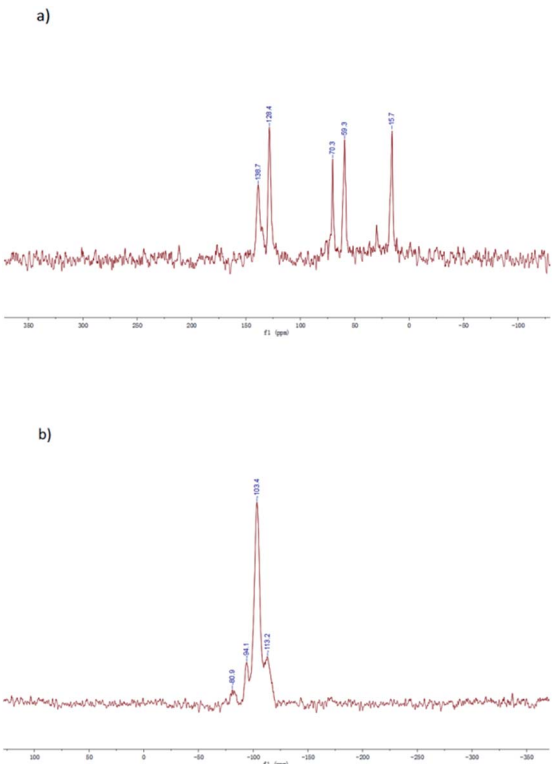

Fig. 2 ^{13}C CP/MAS NMR (a) and ^{29}Si CP/MAS NMR (b) of SBA-15.

Table 1 Properties of the as-synthesized SBA-15 and Pd/SBA-15

Entry	Materials	S_{BET}[a] (m^2 g^{-1})	PV[b] (cm^3 g^{-1})	Pore width (nm)	Contents of Pd[c] (wt%)
1	SBA-15	718	1.20	6.4	—
2	Pd/SBA-15	633	0.92	6.3	1.07

[a] Surface area calculated from the adsorption isotherms using the BET equation. [b] Total pore volume calculated from the nitrogen adsorption at $P/P_0 = 0.99$. [c] Determined by ICP-AES.

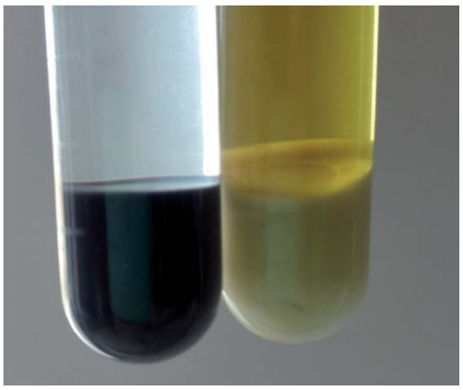

Fig. 3 Image of the as-synthesized Pd/SBA-15 catalyst after centrifugation. Vinyl-functionalized SBA-15 (left) and SBA-15 (right) were used as supports, respectively.

and then with ethanol (50 mL) three times. The solid was dried at 323 K in vacuum overnight to afford Pd/SBA-15.

SBA-15 without vinyl-supported Pd was prepared using the same method, but using SBA-15 (0.50 g) instead of vinyl-functionalized SBA-15.

Characterization of the catalysts

Fourier transform infrared (FT-IR) spectra were collected on a Bruker Tensor 27 FT-IR spectrometer in KBr media. The samples were thoroughly dried before the measurements.

X-ray powder diffraction (XRD) patterns were obtained using a Bruker D8 Advance powder diffractometer with Cu Kα radiation ($\lambda = 0.15418$ nm).

The microstructure of the materials was examined by transmission electron microscopy (TEM) on a Fei Tecnai G2 F20 electron microscope.

N_2 physical adsorption/desorption measurements were carried out at liquid nitrogen temperature on an Autosorb-1 Quantachrome instrument. The samples were pre-degassed at 120 °C for about 12 h to remove water and other physical adsorbed species.

The solid-state NMR spectra were obtained on a Bruker 400 MHz WB solid-state NMR spectrometer.

Inductively coupled plasma atomic emission spectroscopy (ICP-AES) was conducted on an Agilent 725 device.

X-ray photoelectron spectroscopy (XPS) measurements were done in a Thermo Fisher K-alpha using an Al Kα (1486.6 eV) radiation source and a chamber pressure lower than 5×10^{-10} mbar.

Experimental procedure and analysis of the products

Catalytic reactions. The catalytic reactions were performed in a 25 mL Schlenk tube. In a typical experiment, an ethanol solution of the substrates (4 mL, 0.25 mol L^{-1}), decane (100 mg), Pd/SBA-15 (10.0 mg) and a magnetic dipole were put into the tube. Then, the tube was evacuated and put in a 313 K oil bath with a magnetic agitator. Then, 1 atm of H_2 was introduced into the tube and the magnetic agitator was set to 1200 rpm to start the reaction. The pressure was kept at 1 atm by connecting

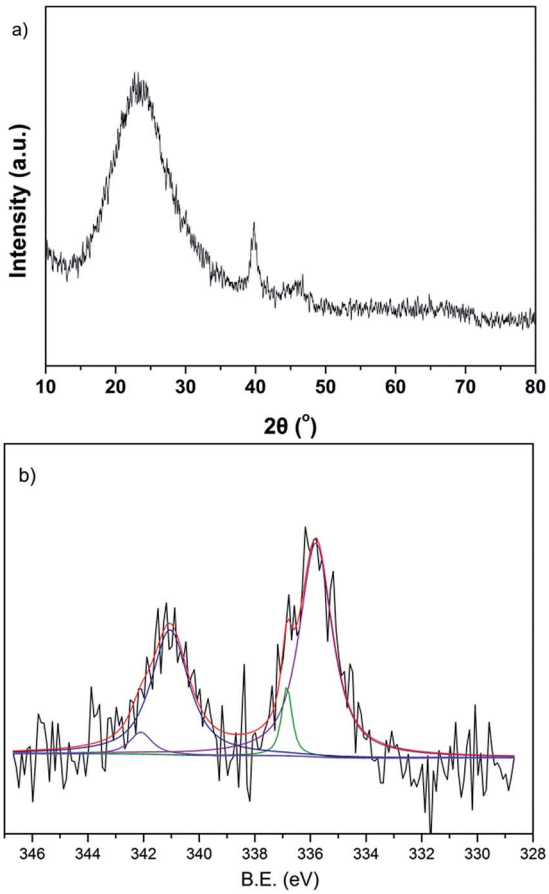

Fig. 4 XRD patterns (a) and XPS spectra (b) of Pd/SBA-15.

the tube to a balloon filled with H_2. Samples were taken at regular intervals and used for gas chromatography analysis.

After reaction, the catalyst was centrifuged and washed with ethanol three times. Then, the catalysts were dried at 323 K in a vacuum overnight and then used for the cyclic tests.

Analysis of the products. The products were identified using an Agilent 6890N GC/5973MS instrument as well as by comparison with the retention times to the corresponding standards in GC. The quantitative analysis was conducted using an Agilent 7890A instrument equipped with an autosampler and a flame ionization detector. The reaction mixtures were separated on an HP-5 capillary column (30 m × 530 μm × 1.5 μm). The temperature of the column was initially kept at 333 K for 3 min, and then was increased at a rate of 20 K min^{-1} to 493 K and kept there for 5 min. Decane was used as the internal standard. The conversion and selectivity of the main products are evaluated below:

$$\text{Conversion } (\%) = \left(1 - \frac{\text{moles of substrate}}{\text{moles of substrate loaded initially}}\right) \times 100\%$$

$$\text{Selectivity } (\%) = \frac{\text{moles of products}}{\text{moles of substrate converted}} \times 100\%$$

Results and discussion

Characterization of the catalysts

Vinyl-functionalized SBA-15 was obtained through the co-polymerization method using P123 as a template agent and tetraethoxysilane (TEOS) as well as vinyltriethoxysilane (VTEO) as the silicon sources according to the literature.[33–36] The N_2 adsorption/desorption isotherms of the as-synthesized SBA-15 showed characteristics of typical type IV physisorption isotherms, according to IUPAC classifications,[37] indicating a mesoporous structure (Fig. 1). SBA-15 had a surface area of 718 $m^2\ g^{-1}$ with an average pore width of 6.4 nm (Table 1), which was in agreement with the results from the TEM analysis (Fig. 5a). The small-angle XRD patterns (Fig. S2†) showed a high (100) peak around $2\theta = 1.2°$ and two weak peaks at the 2θ range between 1.5° and 2.0°, corresponding to the (110) and (200) planes, respectively.[6] The observation of these planes indicates the existence of an ordered two-dimensional (2D) hexagonal structure.

The solid-state ^{29}Si CP/MAS NMR spectrum of vinyl-functionalized SBA-15 is shown in Fig. 2a. The chemical shifts at −113.2 ppm, −103.4 ppm and −94.1 ppm correspond to the different Si environments of $Si(OSi)_4$ [Q^4], $HOSi(OSi)_3$ [Q^3] and $(HO)_2Si(OSi)_2$ [Q^2], respectively.[38] Moreover, a chemical shift at −80.9 ppm ($RSi(OSi)_3$ [T^3]) was also observed in the spectra.[39] These results proved the presence of an organosilane group (Si–CH=CH_2) in the material, which was further confirmed by the solid-state ^{13}C CP-MAS NMR spectra of vinyl-functionalized SBA-15. As shown in Fig. 2, the chemical shifts at 128.4 and 138.7 ppm are attributed to the carbons of the vinyl group, while the 14 and 60–70 ppm shifts were related to the carbons of P123.[35]

Pd/SBA-15 was prepared by stirring a mixture of vinyl-functionalized SBA-15 and an aqueous solution of $PdCl_2$ at room temperature. After centrifuging, a black solid was obtained, while the yellow liquid became colourless (Fig. 3), which indicated that the $PdCl_2$ had been reduced to Pd(0). As a contrast, when SBA-15 with no surface-bonded vinyl was used

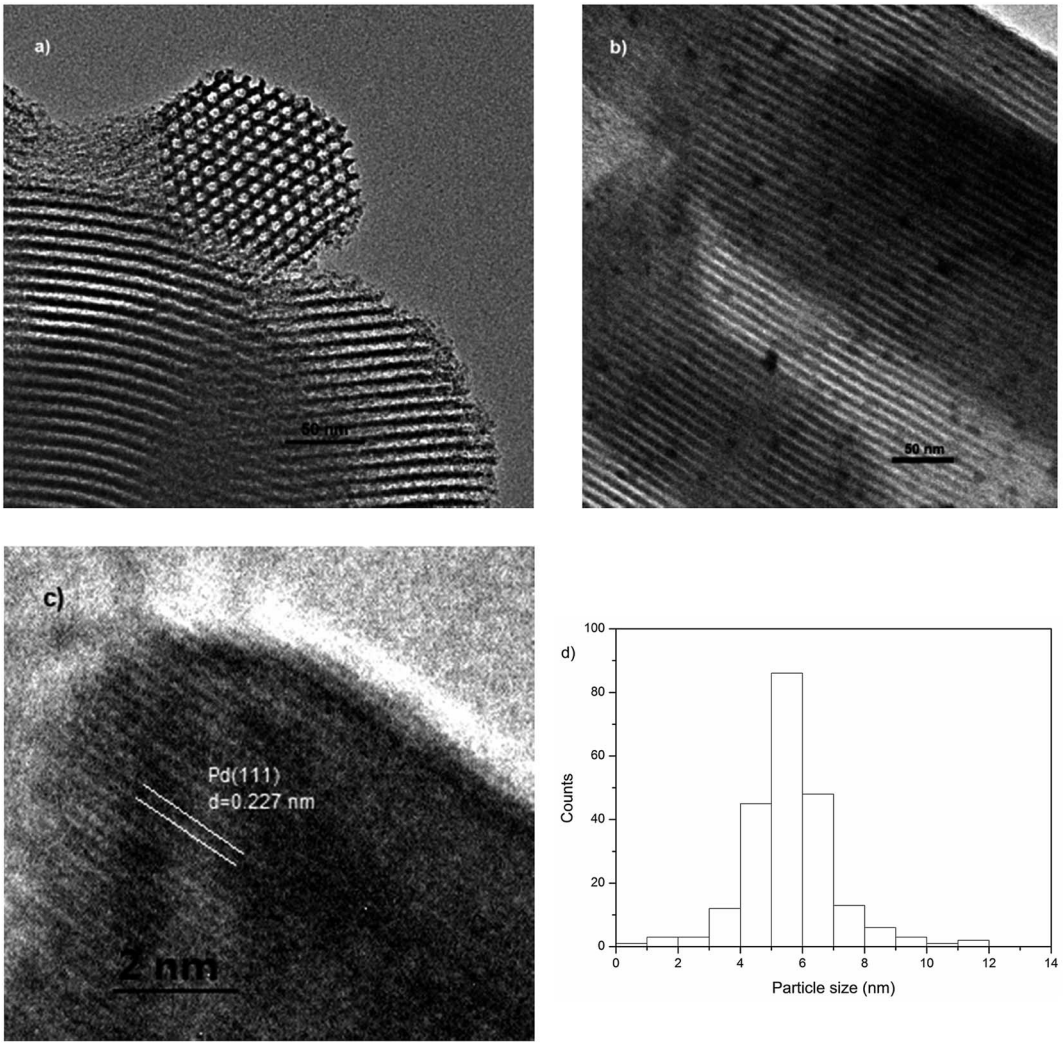

Fig. 5 TEM images of the as-synthesized SBA-15 (a) and Pd/SBA-15 (b). HRTEM image of the Pd nanoparticles (c). Particle-size distribution of Pd/SBA-15 (d).

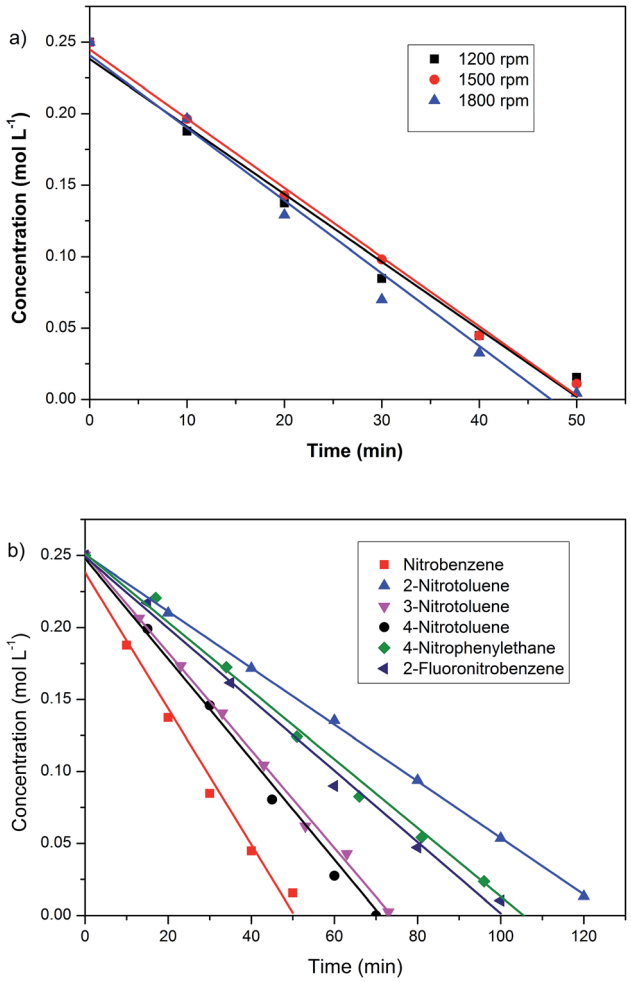

Fig. 6 Influence of the rotation rate (a) and the time–concentration course for the hydrogenation of aromatic nitro compounds (b). Reaction conditions: Pd/SBA-15 (10.0 mg), substrates (1 mmol), ethanol (4 mL), decane (100 mg), 313 K, 1 atm H_2; rotation rate 1200 rpm for (b).

instead, the liquid remained yellow and the solid did not turn black (Fig. 3). This phenomenon illustrated the crucial role of vinyl in the preparation of Pd/SBA-15. The N_2 adsorption/desorption isotherms (Fig. 1) and the intensity of the diffraction peaks corresponding to the (100), (110) and (200) planes in the small-angle XRD patterns (Fig. S2†) gave no indication of obvious changes, which indicates that the mesoporous structure of SBA-15 was well kept after the introduction of palladium. However, all the diffraction peaks were shifted to higher angles in the small-angle XRD patterns (Fig. S2†) and the surface area and average pore width decreased to 633 m^2 g^{-1} and 6.3 nm, respectively, (Table 1) due to the introduction of Pd.

The presence of metallic palladium was characterised by the XRD pattern as well as by the XPS spectra (Fig. 4). The wide peak centred at $2\theta = 23°$ was caused by the amorphous silica composition of SBA-15. The weak peaks at $2\theta = 40°$ and 46° corresponded to the (111) and (200) crystalline planes of Pd. These results confirmed that the $PdCl_2$ had already been reduced to Pd. The XPS spectrum was also used to investigate the oxidation state of palladium. The binding energy peaks of 335.8 eV and 341.1 eV corresponded to Pd $3d_{5/2}$ and Pd $3d_{3/2}$,[40] giving the hints of Pd(0). Additionally, weak binding energy peaks at 336.9 eV and 342.1 eV were observed, corresponding to $3d_{5/2}$ and $3d_{3/2}$ of Pd(II).[36] This should be recommended by the oxidation of Pd(0) in an air atmosphere.

The distribution of palladium on the SBA-15 could be revealed by recording the TEM images of Pd/SBA-15 (Fig. 5). The mesoporous structure of SBA-15 was untouched after the introduction of palladium. The palladium nanoparticles were distributed on SBA-15 with a narrow size distribution of about 5–6 nm due to the application of surface-bonded vinyl as the reducing agent. Palladium nanoparticles were produced through the reduction of $PdCl_2$ by the vinyl group. Once the vinyl nearby was exhausted, the palladium nanoparticles could not be enlarged as there were no reducing agents nearby.

Hydrogenation of nitroarenes

The hydrogenation of aromatic nitro compounds was used to test the hydrogenation ability of the as-synthesised Pd/SBA-15. Initially, the hydrogenation of nitrobenzene was conducted as the model reaction. The reaction was first performed at different rotation rate to exclude the effects of diffusion. The rotation rate had little influence on the reaction rate between

Table 2 Comparison of various catalysts in the reduction of nitrobenzene under different conditions

Entry	Catalysts	Metal loading (wt%)	T (K)	Pressure (MPa)	Yield (%)	TOF[a] (h^{-1})	Ref.
1	Ni–$NiFe_2O_4$/carbon	—	423	1	~100	—	41
2	Au/SiO_2-org	1.0	413	4	99	400	42
3	Pt–NHC	67	303	0.1	99	2433	43
4	Ru/RGO	3.4	383	2	99	793	44
5	SS-Pd[b]	0.5	323	—	98	50	45
6	Fe_3O_4–NH_2–Pd	8.43	r.t.	0.1	99	83	46
7	Pd/HAM@γ-AlOOH	7.20	r.t.	0.1	~100	99	47
8	Pd@Fe_3O_4	0.87	r.t.	0.1	99	493	48
9	Pd/PMO–SBA-15	1.5	318	0.1	54	766	6
10	Pd/SBA-15	1.07	313	0.1	98	1124	This work

[a] The TOF was calculated by the data provided in the reference based on the consumption of nitrobenzene. [b] $NaBH_4$ was used as the reducing agent.

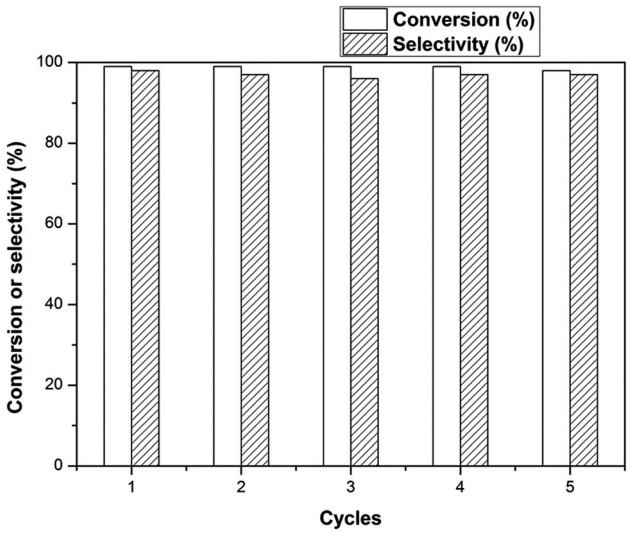

Fig. 7 The cycle experiments for the hydrogenation of nitrobenzene. Reaction conditions: Pd/SBA-15 (10.0 mg), nitrobenzene (1 mmol), ethanol (4 mL), decane (100 mg), 313 K, 1 atm H_2, 60 min.

1200 and 1800 rpm. Thus, the effect of diffusion was negligible above 1200 rpm (Fig. 6a). The reaction showed zero-order kinetics, as the graphs of concentration against time gave good straight-line plots (Fig. 6b). This suggests that the concentration of nitrobenzene had no influence on the reaction rate. Thus, the reaction rate was determined by the amount of active sites at the reaction conditions. The Pd/SBA-15 catalyst showed high activity and selectivity for the hydrogenation of nitrobenzene. The TOF was 1124 h^{-1} at 313 K and 1 atm H_2 with over 95% selectivity of aniline. A comparison of the activity of various catalysts reported in the literature with the as-synthesised Pd/SBA-15 is exhibited in Table 2. Catalysts containing Pd, Ru, Pt and Ni were effective for the hydrogenation of nitrobenzene in H_2. It can be seen that the Pd/SBA-15 catalyst reported in this manuscript had a very high TOF compared to the other reported systems.

The Pd/SBA-15 catalyst was also effective for the hydrogenation of aromatic nitro compounds, including nitrobenzene with fluorous groups (Fig. 6b). The corresponding aromatic amino compounds were obtained with a selectivity of more than 90%, which showed the high selectivity of the catalyst. All the reactions showed zero-order kinetics, and a steric effect was also observed. The TOF was 805 h^{-1} for the hydrogenation of 3-nitrotoluene, which was very close to the TOF (827 h^{-1}) for the hydrogenation of 4-nitrotoluene, while the TOF for 2-nitrotoluene was 468 h^{-1} (Table S1†). This decrease in activity should be due to the steric effect. The steric hindrance of 2-nitrotoluene was bigger than that of 3-nitrotoluene and 4-nitrotoluene.

The reusability of the catalysts was measured by cyclic tests. The catalysts were centrifuged and washed with ethanol three times after each reaction. After drying at 323 K under vacuum, the catalysts were used for the next run. The results are shown in Fig. 7. The conversion and selectivity kept almost constant in all the five cycles and the yield of aniline was over 95%. The results showed that the catalysts were very stable under the reaction conditions.

Conclusions

In summary, we synthesized a type of highly efficient Pd/SBA-15 catalyst by employing surface-bonded vinyl as a reductant and tested its application in the hydrogenation of aromatic nitro compounds. It is noteworthy that the surface-bonded vinyl was an effective reductant for $PdCl_2$ in water compared to the preparation of Pd/SBA-15. Moreover, this Pd/SBA-15 catalyst had a narrow particle-size distribution of around 5–6 nm and was effective for the hydrogenation of aromatic nitro compounds under mild conditions. This work provides a new method for the preparation of supported palladium nanoparticles and more research related to this subject are in progress in our laboratory.

Acknowledgements

This work was supported by the Intercollegiate Key Scientific Research Projects of Henan Province (15A150065 and 15A150018).

Notes and references

1 A. Corma, H. García and F. X. Liabrés i Xamena, *Chem. Rev.*, 2010, **110**, 4606–4655.
2 M. J. Climent, A. Corma, S. Iborra and M. J. Sabater, *ACS Catal.*, 2014, **4**, 870–891.
3 M. Zhao, S. Ou and C. D. Wu, *Acc. Chem. Res.*, 2014, **47**, 1199–1207.
4 H. Feng, X. Zhu, R. Chen, Q. Liao, J. Liu and L. Li, *Chem. Eng. J.*, 2016, **306**, 1017–1025.
5 Y. Wang, J. Yao, H. Li, D. Su and M. Antonietti, *J. Am. Chem. Soc.*, 2011, **133**, 2362–2365.
6 C. Liu, R. Tan, N. Yu and D. Yin, *Microporous Mesoporous Mater.*, 2010, **131**, 162–169.
7 Y.-Z. Xiang, L.-N. Kong, C.-S. Lu, L. Ma and X.-N. Li, *React. Kinet., Mech. Catal.*, 2010, **100**, 227–235.
8 C. G. Morales-Guio, I. Yuranov and L. Kiwi-Minsker, *Top. Catal.*, 2014, **57**, 1526–1532.
9 V. Udayakumar and A. Pandurangan, *RSC Adv.*, 2015, **5**, 78719–78727.
10 E. van Ryneveld, A. S. Mahomed, P. S. van Heerden and H. B. Friedrich, *Catal. Lett.*, 2011, **141**, 958–967.
11 Y. Shao, Q. Xia, X. Liu, G. Lu and Y. Wang, *ChemSusChem*, 2015, **8**, 1761–1767.
12 M. G. Musolino, F. Mauriello, C. Busacca and R. Pietropaolo, *Top. Catal.*, 2015, **58**, 1077–1084.
13 Q. Meng, C. Qiu, G. Ding, J. Cui, Y. Zhu and Y. Li, *Catal. Sci. Technol.*, 2016, **6**, 4377–4388.
14 Q. Meng, H. Zheng, Y. Zhu and Y. Li, *J. Mol. Catal. A: Chem.*, 2016, **421**, 76–82.
15 P. Wang, G. Zhang, H. Jiao, L. Liu, X. Deng, Y. Chen and X. Zheng, *Appl. Catal., A*, 2015, **489**, 188–192.

16 Y. Zhao, R. Tang and R. Huang, *Catal. Lett.*, 2015, **145**, 1961–1971.
17 P. Verma, Y. Kuwahara, K. Mori and H. Yamashita, *J. Mater. Chem. A*, 2015, **3**, 18889–18897.
18 N. Noori, M. Nikoorazm and A. Ghorbani-Choghamarani, *J. Porous Mater.*, 2016, **23**, 1467–1481.
19 Y. Hao, S. Wang, Q. Sun, L. Shi and A.-H. Lu, *Chin. J. Catal.*, 2015, **36**, 612–619.
20 Y. Pan, B. Yuan, Y. Li and D. He, *Chem. Commun.*, 2010, **46**, 2280–2282.
21 J. Liu, G. Hu, Y. Yang, H. Zhang, W. Zuo, W. Liu and B. Wang, *Nanoscale*, 2016, **8**, 2787–2794.
22 X. Bian, K. Guo, L. Liao, J. Xiao, J. Kong, C. Ji and B. Liu, *Talanta*, 2012, **99**, 256–261.
23 J. P. Ford, J. G. Immer and H. H. Lamb, *Top. Catal.*, 2012, **55**, 175–184.
24 S. Ding, Q. Yan, H. Jiang, Z. Zhong, R. Chen and W. Xing, *Chem. Eng. J.*, 2016, **296**, 146–153.
25 L. Kong, X. Lu, X. Bian, W. Zhang and C. Wang, *Langmuir*, 2010, **26**, 5985–5990.
26 F. Zhang, J. Yin, W. Chai and H. Li, *ChemSusChem*, 2010, **3**, 724–727.
27 S. C. Mitchell and R. H. Waring, *Ullmanns Encyclopedia of Industrial Chemistry*, Wiley-VCH, Germany, 2000.
28 V. Pandarus, R. Ciriminna, F. Béland and M. Pagliaro, *Adv. Synth. Catal.*, 2011, **353**, 1306–1316.
29 H. K. Kadam and S. G. Tilve, *RSC Adv.*, 2015, **5**, 83391–83407.
30 R. Begum, R. Rehan, Z. H. Farooqi, Z. Butt and S. Ashraf, *J. Nanopart. Res.*, 2016, **18**, 231–244.
31 V. S. Marakatti and S. C. Peter, *New J. Chem.*, 2016, **40**, 5448–5457.
32 P. Lara and K. Philippot, *Catal. Sci. Technol.*, 2014, **4**, 2445–2465.
33 D. Y. Zhao, J. L. Feng, Q. S. Huo, N. Melosh, G. H. Fredrickson, B. F. Chmelka and G. D. Stucky, *Science*, 1998, **279**, 548–552.
34 Y. Yang, Z. Du, Y. Huang, F. Lu, F. Wang, J. Gao and J. Xu, *Green Chem.*, 2013, **15**, 1932–1940.
35 Y. Wang, B. Zibrowius, C. M. Yang, B. Spliethoff and F. Schuth, *Chem. Commun.*, 2004, 46–47.
36 B. G. Park, J. Park, W. Guo, W. J. Cho and C. S. Ha, *Stud. Surf. Sci. Catal.*, 2003, **146**, 489–492.
37 A. Wach, M. Drozdek, B. Dudek and P. Kuśtrowski, *Surf. Interface Anal.*, 2014, **46**, 1021–1027.
38 S. Shi, M. Wang, C. Chen, F. Lu, X. Zheng, J. Gao and J. Xu, *RSC Adv.*, 2013, **3**, 1158–1164.
39 M. Wang, F. Wang, J. Ma, C. Chen, S. Shi and J. Xu, *Chem. Commun.*, 2013, **49**, 6623–6625.
40 M. Brun, A. Berthet and J. C. Bertolini, *J. Electron Spectrosc. Relat. Phenom.*, 1999, **104**, 55–60.
41 W. J. Liu, K. Tian and H. Jiang, *Green Chem.*, 2015, **17**, 821–826.
42 X. Tan, Z. Zhang, Z. Xiao, Q. Xu, C. Liang and X. Wang, *Catal. Lett.*, 2012, **142**, 788–793.
43 P. Lara, A. Suárez, V. Collière, K. Philippot and B. Chaudret, *ChemCatChem*, 2014, **6**, 87–90.
44 G. Fan, W. Huang and C. Wang, *Nanoscale*, 2013, **5**, 6819–6825.
45 A. K. Shil, D. Sharma, N. R. Guha and P. Das, *Tetrahedron Lett.*, 2012, **53**, 4858–4861.
46 F. Zhang, J. Jin, X. Zhong, S. Li, J. Niu, R. Li and J. Ma, *Green Chem.*, 2011, **13**, 1238–1243.
47 M. Tian, X. Cui, C. Dong and Z. Dong, *Appl. Surf. Sci.*, 2016, **390**, 100–106.
48 A. J. Amali and R. K. Rana, *Green Chem.*, 2009, **11**, 1781–1786.